A&A 571, A99 (2014)
DOI: 10.1051/0004-6361/201322301

Astronomy & Astrophysics

A mass threshold in the number density of passive galaxies at $z \sim 2$

V. Sommariva[1], A. Fontana[1], A. Lamastra[1], P. Santini[1], J. S. Dunlop[3], M. Nonino[2], M. Castellano[1], H. Ferguson[4], R. J. McLure[3], A. Galametz[1], M. Giavalisco[5], A. Grazian[1], Y. Lu[6], N. Menci[1], A. Merson[7], D. Paris[1], L. Pentericci[1], R. Somerville[4], T. Targett[3], and A. M. Koekemoer[8]

[1] INAF – Osservatorio Astronomico di Roma, Via Frascati 33, 00040 Monteporzio, Italy
e-mail: veronica.sommariva@oa-roma.inaf.it
[2] INAF – Osservatorio Astronomico di Trieste, Via G.B. Tiepolo 11, 34131 Trieste, Italy.
[3] SUPA, Institute for Astronomy, University of Edinburgh, Royal Observatory, Edinburgh, EH9 3HJ, UK
[4] Space Telescope Science Institute, 3700 San Martin Dr., Baltimore, MD 21218, USA
[5] Astronomy Department, University of Massachusetts, Amherst, MA 01003, USA
[6] Kavli Institute for Particle Astrophysics and Cosmology, 452 Lomita Mall, Stanford, CA 94305-4085
[7] Department of Physics and Astronomy, University College London, Gower Street, London WC1E 6BT, UK
[8] Space Telescope Science Institute, 3700 San Martin Drive, Baltimore, MD 21218, USA

Received 17 July 2013 / Accepted 1 September 2014

ABSTRACT

The process that quenched star formation in galaxies at intermediate and high redshifts is still the subject of considerable debate. One way to investigate this puzzling issue is to study the number density of quiescent galaxies at $z \simeq 2$ and its dependence on mass. Here we present the results of a new study based on very deep K_s-band imaging (with the HAWK-I instrument on the VLT) of two HST CANDELS fields (the UKIDSS Ultra-deep survey (UDS) field and GOODS-South). The new HAWK-I data (taken as part of the HUGS VLT Large Program) reach detection limits of $K_s > 26$ (AB mag). We have combined this imaging with the other ground-based and HST data in the CANDELS fields to select a sample of passively-evolving galaxies in the redshift range $1.4 < z < 2.5$ (via the pBzK color-based selection criterion). Thanks to the depth and wide area coverage of our imaging, we have been able to extend the selection of quiescent galaxies to a magnitude fainter than previous analyses. Through extensive simulations we demonstrate, for the first time, that the observed turnover in the number of quiescent galaxies at $K \geq 22$ is not due to incompleteness, but is real. This has enabled us to establish unambiguously that the number counts of quiescent galaxies at $z \simeq 2$ flatten and slightly decline at magnitudes fainter than $K_s \sim 22$ (AB mag.), in contrast to the number density of star-forming galaxies, which continues to rise to fainter magnitudes. We show that this trend corresponds to a stellar mass threshold $M_* \simeq 10^{10.8}\ M_\odot$ below which the mechanism that halts the star formation in high-redshift galaxies seems to be inefficient. We also show that, while pBzK galaxies at $K < 23$ are in the redshift range $1.4 < z < 2.5$, as expected, at $K > 23$ a higher redshift population of $z \simeq 3$ pBzK galaxies is detected and dominates the counts at the faintest magnitudes. Finally, we compare the observed pBzK number counts with those of quiescent galaxies extracted from four different semi-analytic models. We find that only two of these models reproduce the observed trend in the number counts, even qualitatively, and that none of the models provides a statistically acceptable description of the number density of quiescent galaxies at these redshifts. We conclude that the mass function of quiescent galaxies as a function of redshift continues to present a key and demanding challenge for proposed models of galaxy formation and evolution.

Key words. Galaxy: fundamental parameters – galaxies: high-redshift

1. Introduction

The cessation or "quenching" of star formation activity in galaxies at high and intermediate redshifts is one of the key events in the history of galaxy evolution and is one that is not easily explained in the context of hierarchical growth within a ΛCDM cosmology. While it is now established that the (apparently fairly rapid) termination of star formation in some subset of the galaxy population only a few billion years after the Big Bang must be attributed to some aspect of baryonic physics, the relevant process remains a matter of debate, with opinion divided over whether the key mechanism is feedback from an active galactic nucleus (AGN), feedback from star formation itself, or termination of the gaseous fuel supply (e.g., due to the difficulty of cool gas penetrating to the center of a massive halo because of shock heating). Better observational constraints on the prevalence and properties of quiescent galaxies at high redshift are therefore urgently required in order to constrain models of galaxy formation and evolution over cosmic history.

One main goal is to better establish the mass dependence of star-formation quenching. A number of lines of evidence suggest that this process appears "anti-hierarchical" in the sense that it is the most massive galaxies that cease star formation at the earliest times, leading ultimately to the present-day Universe in which the most massive elliptical galaxies appear to be the oldest. However, because less-massive passive galaxies are hard to detect and isolate at high redshift (especially at optical wavelengths), it has proved difficult to establish the definitive mass dependence of the number density of passive galaxies at the crucial epoch corresponding to $z \simeq 2$. The primary aim of this study is to clarify this situation via new deep multi-frequency imaging data.

Several methods have been developed to efficiently select passively evolving galaxies at high redshift based on color

criteria. In recent years, the most extensively used selection technique has been the BzK color–color selection introduced by Daddi et al. (2004). They show that galaxies in the redshift range $1.4 < z < 2.5$ fall into a specific area of the $(B-z)/(z-K)$ diagram and demonstrate that galaxies can be easily separated into star-forming (sBzK) and passively evolving (pBzK) classes. This technique also has the advantage of not being biased by the presence of dust; the reddening vector in the BzK plane is parallel to the BzK selection line, making this criterion relatively immune to dust content.

A number of studies have used the BzK criterion to constrain the properties of star-forming and passive galaxies at $z \simeq 2$. For example, Kong et al. (2006) present K_s-selected samples of BzK galaxies over two fields: a $\simeq 920$ arcmin^2 field (with $K_{s;AB} < 20.8$) and a $\simeq 320$ arcmin^2 field (to $K_{s;AB} \simeq 21.8$). They particularly concentrated their analysis on the clustering properties of BzK galaxies, and conclude that the pBzK galaxies are more clustered than the sBzK galaxies. Meanwhile, Lane et al. (2007) combined the first release of the near-infrared UKIRT Infrared Deep Sky Survey (UKIDSS) Ultra-Deep Survey (UDS; Lawrence et al. 2007) with optical photometry from Subaru imaging. By comparing the commonly used selection techniques for galaxies at intermediate redshift, they conclude that the brightest distant red galaxies (DRG) have spectral energy distributions (SED) that are consistent with dusty star-forming galaxies at $z \simeq 2$. Moreover, they observed an interesting turnover in their derived number counts of pBzK galaxies at $K \simeq 21$, suggesting an absence of high-redshift passive galaxies at lower luminosities. Grazian et al. (2007), instead, focused on the overlap between DRG and BzK galaxies, discussing their relative contribution to the overall stellar mass density.

The galaxy population in the UKIDSS UDS field was also studied by Hartley et al. (2008), in order to measure the clustering properties, number counts, and the luminosity function of a sample of star-forming and quiescent BzK galaxies with a limiting magnitude $K_{s;AB} < 23$. The number counts they derived for the passive objects exhibit a flattening at $K_s \simeq 21$ and an apparent turnover at $K_s \simeq 22$: they conclude that the former effect is likely to be real, while the latter is probable but remains uncertain. More recently, McCracken et al. (2010) have presented number counts and clustering properties for a sample of pBzK galaxies with $K_s < 23$, selected over a significantly larger area than previous studies (2 deg^2 in the COSMOS field). They also found some evidence of a turnover in the number counts of quiescent galaxies, around $K_s \simeq 22$.

It is interesting to notice that similar conclusions have already been reached by other papers using different techniques. For instance, De Lucia et al. (2007) used a combination of photometric and spectroscopic data to study the evolution of cluster environment over a wide range of cosmic time, from redshift 0.4 to 1. They found a significant deficit of low-mass, faint red galaxies going to high redshift. A similar conclusion, i.e., the truncation of the red sequence at faint magnitude for high redshift galaxies, was confirmed by other authors, such as Kodama et al. (2004) and Andreon et al. (2011). A decline in the number density of the quiescent population at faint magnitudes was also observed in the H_{160}-band by Stutz et al. (2008). More recently, Ilbert et al. (2013) have presented galaxy stellar mass functions and stellar mass densities for star-forming and quiescent galaxies in the redshift range $0.2 < z < 4$ using the UltraVISTA DR1 data release. They studied the stellar mass function for both star-forming and quiescent galaxies and find that the number density of massive, quiescent galaxies is relatively unchanged out to high redshift. They interpret this evidence as a direct consequence of star formation being drastically reduced or quenched when a galaxy becomes more massive than $M > 10^{10.7-10.9}\,M_\odot$. This result is consistent with the one presented in Muzzin et al. (2013), who also computed the stellar mass function for quiescent galaxies using the UltraVISTA data. In general, dedicated analyses of the evolution of "Red&Dead" galaxies show an evolution in the fraction of red galaxies (e.g., Fontana et al. 2009; Brammer et al. 2011) that decreases as redshift increases.

The use of the BzK selection method for finding passively evolving galaxies has the distinct advantages of being relatively easy to perform on data, of being easily and self-consistently reproducible on mock catalogs derived from theoretical simulations, and being relatively well tested with spectroscopic follow-up. However, it is crucial to stress that the success rate of the BzK selection strongly depends on the availability of deep imaging at both optical and near-infrared wavelengths. All the above-mentioned surveys were limited both by the depth of the near-infrared data and by the relative depth of the imaging in the bluer bands. The robust detection of passively evolving BzK galaxies requires the proper measure of a color term as large as $B-K \simeq 7$. If the B-band imaging is of limited depth, the clean selection of pBzK galaxies cannot reach the faint K-band limits where the bulk of the population is expected to lie, and the observed number counts are severely prone to errors due to incompleteness and noise. Because of these limitations, the existence of a turnover in the observed number counts of quiescent galaxies at $z \simeq 2$ has yet to be firmly established.

In this paper, we use a combination of wide-field and deep optical and infrared images that allow us to robustly select a sample of passively evolving galaxies at $z \simeq 2$ to $K_s \simeq 25$ and to explore the dependence of the number density of these quiescent objects as a function of luminosity or, equivalently, stellar mass. The data have been acquired in the context of the CANDELS HST (Grogin et. al 2011; Koekemoer et al. 2011) and HUGS VLT (Fontana et al. 2014) surveys, which deliver a unique combination of area and depth in the B, z, and K_s bands. With this unique sample, we study the number counts of the BzK galaxy population, and in particular we focus on the quiescent population to provide improved constraints on the nature of the physical processes involved in the quenching of star formation.

The paper is organized as follows. In Sect. 2 we describe the data and the multiwavelength catalog for the UDS and GOODS-S fields, in Sect. 3 we provide an updated view of the properties of faint BzK galaxies as obtained by the unique CANDELS data set, and in Sect. 4 we present the simulations performed to quantify the incompleteness of the observed sample. A reader less interested in the technical details may go directly to Sect. 5, where we present the crucial result of the paper, i.e. the luminosity and mass distribution of pBzK galaxies, and to Sect. 6, where we compare our results with the predictions of various semi-analytical models (SAM) of galaxy formation. Finally, a discussion of our results and a summary of our main conclusions is presented in Sect. 7.

All magnitudes utilized in the paper are in the AB system (Oke 1974) and in a standard cosmological model ($H_0 = 70$ km s^{-1}/Mpc, $\Omega_M = 0.3$, and $\Omega_\Lambda = 0.7$).

2. Data

2.1. Imaging data

The present paper is based on data collected over the CANDELS pointings of the UDS and the GOODS-S fields. Both these

$\simeq$200 arcmin^2 fields have been observed in many broad bands in recent years, including WFC3/IR and ACS with the *Hubble* Space Telescope (HST), as a part of CANDELS HST Treasury Project (Grogin et al. 2011; Koekemoer et al. 2011). Additional ultradeep images from the U to the mid-infrared *Spitzer* bands are also available. A complete description of the imaging data available in these fields, along with the procedure adopted for catalog extraction, are given in Galametz et al. (2013, G13 in the following) for UDS and in Guo et al. (2013, GUO13 in the following) for GOODS-S, respectively.

Since this work makes crucial use of the B, z, and K bands to select passive galaxies, we briefly summarize the properties of these images, including new imaging data in the B and K bands that were recently collected with VLT that are not included in the aforementioned catalog papers.

In the K band, the two fields have been imaged by the High Acuity Wide field K-band Imager (HAWK-I) on the European Southern Observatory's Very Large Telescope (VLT) as part of the HUGS survey (an acronym for HAWK-I UDS and GOODS-S survey). This program has delivered very deep images in the K_s band over both fields, reaching 5-σ detection limits fainter than $K_s \simeq 26$. We refer to Fontana et al. (2014) for a complete description of the HUGS survey. The K_s band of HAWK-I will be referred to simply as the K-band in the rest of this paper.

For UDS, the final K-band photometry is already included in the G13 catalog. The whole UDS field is covered with three different pointings. Their seeing is $0.37'' - 0.43''$ and the corresponding limiting magnitudes are $m_{\rm lim}(K) \simeq 26$, $m_{\rm lim}(Y) \simeq 26.8$ (5σ in one FWHM) or $m_{\rm lim}(K) \simeq 27.3$, $m_{\rm lim}(Y) \simeq 28.3$ (1σ per arcsec^2). In GOODS-S, we use here the final HUGS image, which is considerably deeper than the image used in GUO13. The whole field was covered with six (partly overlapping) pointings for a total exposure time in the K band (summed over the six pointings) of 107 h. Because of the complex geometry, this corresponds to an exposure of 60–80 h in the central area (the one covered by CANDELS "Deep") and 12–20 h in the rest (the CANDELS "Wide" area). The final average seeing is remarkably good and constant, with four pointings at $0.38''$ (notably including the two deepest) and two at $0.42''$. In the finally stacked images, the limiting magnitudes in the deepest area are $m_{\rm lim}(K) \simeq 27.8$ (5σ in one FWHM) or $m_{\rm lim}(K) \simeq 28.3$, $m_{\rm lim}(Y) \simeq 28.3$ (1σ per arcsec^2).

The B and z' images in the UDS were obtained with Subaru/Suprime-Cam (see Furusawa et al. 2008). The Subaru optical data cover the full CANDELS UDS field, and the 5σ limiting magnitudes (computed in 1 FWHM of radius) are 28.38 in B and 26.67 in $z'(G13)$.

Another crucial data set in this context is a recent ultradeep B-band image obtained with VIMOS on VLT for GOODS-S (Nonino et al. in prep.). Here the average seeing is $0.89''$. With a VLT/VIMOS total integration time of 24 h, the final mosaics have a median point spread function (PSF) of 0.85 arcsec FWHM and reach $B = 28.4$ at 5σ. They are thus considerably deeper than the available ACS $F435W$ data (the latest V2.0 version released by the GOODS Team reaches a 5σ limit of $F435W \simeq 26.9$). We use this VIMOS B-band image in the following. As for the GOODS-S z band, we used the $F850LP$ image originally obtained in the GOODS program (Giavalisco et al. 2004) and then augmented by subsequent observations. Guo et al. (2013) report a 5σ limit of $m_{\rm AB} = 28.55$ in a small aperture of radius $0.09''$.

While the B, z, and K bands are crucial for the selecting passive galaxies, we have also utilized the full multicolor data from the U-band to the mid-infrared *Spitzer* bands at various stages in our analysis, both to derive photometric redshifts and to determine the shapes of the SEDs of the selected galaxies. We refer to G13, GUO13, and Fontana et al. (2014) for a complete description of the imaging data set.

2.2. Catalogs

The catalogs used in this paper are those already published in G13 and GUO13, with the only notable difference that we have included the new B and K images, as described below. The adoption of the CANDELS catalogs implies that we rely on the H_{160} band for the detection of galaxies. This choice has the practical benefit that we have been able to use the existing CANDELS catalogs, and it takes full advantage of the depth and the quality of the HST images. Because the H_{160} imaging is still significantly deeper than the K-band imaging, this choice does not affect the definition of the K-selected sample. We have performed an independent detection in the K band and verified that all the objects detected in K are also detected in H band, at least to the magnitude limits we are interested in here.

From the whole H-selected sample, we then selected the objects that fall in the regions where the K band images are exposed well, trimming the outer edges of the images. The remaining areas are 151.08 arcmin^2 in GOODS-S (defined as all pixels of the image having a 1σ magnitude limit >27 in one sq. arcsec) and 178.09 arcmin^2 in UDS (made by pixels with a 1σ magnitude limit >26.5 in one sq. arcsec). The final UDS sample (that is complete to $H \simeq 26$ and extends to $H \simeq 27$) contains 27831 H-selected objects, while the GOODS sample (that is complete to $H \simeq 26.6$ and extends to $H \simeq 28$) contains 31551 H-selected objects.

Colors in the ACS and WFC3/IR bands were measured by running SExtractor in dual-image mode, using isophotal magnitudes (MAG_ISO) for all the galaxies, after smoothing each image with an appropriate kernel to reproduce the resolution of the H_{160} WFC3/IR image. The Template-FITting photometry software TFIT (Laidler et al. 2007) was used to derive the photometry for all the images that have poorer resolution than H_{160} (e.g., B, z', and K). This code uses information (position, profile) of sources measured on a high-resolution image (here H_{160}) as priors to establish the photometry in the lower resolution images. We refer to G13 for a more detailed discussion of the CANDELS UDS multiwavelength catalog. For the new B and K images used here, we applied TFIT exactly as described in G13 and GUO13.

We notice that the TFIT code that we used to measure colors is designed to minimize the effects of blending from nearby sources when extracting the photometry of faint sources in crowded extragalactic fields. The power of TFIT in this context is clearly shown by the simulations presented in Lee et al. (2012), where it is shown that the contamination from nearby sources is minimal even in the case of the $\simeq 3''$ PSF of the *Spitzer* images. The ground–based images on which this analysis is based (B, z, K) have a much smaller PSF, especially in K where the seeing is consistently better than $0.45''$, and we therefore expect possible contaminations to be even smaller. As a further check, we verified that only 5% of galaxies at $K \simeq 23.5$–24 (the most typical objects that we target) have a nearby brighter companion within $2''$, which may be affecting the measured colors. We are therefore confident that our results are not significantly affected by photometric contamination.

We also note that the images used in this analysis are remarkably homogeneous in depth over the area that we use.

Ground–based B and z images have been obtained with imagers with a FOV that is larger than those of CANDELS fields, and the dithering pattern adopted for Hawk–I has ensured proper coverage of the full area. We explicitly verified this by looking at the distributions of the 1σ magnitude limits in the B, z, and K images for our BzK galaxies, and we verified that they are reasonably narrow Gaussian distributions. The remaining inhomogeneities are accounted for in the simulations that we used to evaluate the systematics in our analysis.

To facilitate comparison of our results with previous studies, we wanted our photometric selection criterion to match the original BzK selection introduced in Daddi et al. (2004) as closely as possible. Since the filters used here in both the GOODS-S and UDS fields are not identical to those used in the original BzK paper, we computed the correction term to the colors to account for the different shapes of the filters. Correction terms were computed using synthetic models of Galactic stars and checked against the terms computed with the Bruzual & Charlot (2003, BC03) evolutionary synthesis code. Corrections for the two colors in GOODS-S and for $z-K$ in UDS turned out to be relatively small, nearly always less than 0.05 mag, both between the UDS and GOODS-S filters, as well as in comparison with the original Daddi et al. photometry. The $(B-z)$ color term in UDS turned out to be significantly larger, with a strong linear trend up to $\Delta(B-z)_{\rm UDS-GOODS-S} \simeq \Delta(B-z)_{\rm UDS-Daddi} \simeq -0.3$. We therefore decided to only apply a correction to $(B-z)_{\rm UDS}$, in order to bring it as close as possible to $(B-z)_{\rm GOODS}$, neglecting all the other much smaller color terms. The corrected color is $(B-z)^{\rm corr}_{\rm UDS} = (B-z)_{\rm UDS} + 0.135 \times (B-z)_{\rm UDS} + 0.045$ up to $(B-z)_{\rm UDS} = 2$, and $(B-z)^{\rm corr}_{\rm UDS} = (B-z)_{\rm UDS} + 0.315$ at larger $(B-z)_{\rm UDS}$. Hereafter we apply this correction to data and theroretical models (when computed explicitly in the UDS filter set) and refer to $(B-z)^{\rm corr}_{\rm UDS}$ as $(B-z)_{\rm UDS}$ for simplicity. The final agreement can be visualized in Fig. 1, where we have plotted an identical red dashed line in the two panels that overlaps the stellar loci of the two fields. As can be seen, the consistency of the two calibrations is good.

2.3. The SED fitting

While the selection of passive galaxies is performed using only the BzK bands, we exploit the full multiwavelength catalogs delivered by CANDELS to obtain further information on the targeted galaxies, including photometric redshifts, stellar masses, and other quantities. For all the BzK galaxies without a secure spectroscopic redshift we used the official photometric redshift produced by the CANDELS collaboration. The technique adopted is described in Dahlen et al. (2013), and photometric redshifts for both fields will be made available in forthcoming papers (Dahlen et al., in prep.). For the sample of BzK galaxies with secure spectroscopic redshifts, we find that the scatter between photometric and spectroscopic redshifts is Gaussian-distributed, with a standard deviation $\sigma \sim 0.08$ and a small number of outliers, about 5%.

To compute the physical parameters of the galaxies, we used a SED fitting technique applied to the full multiwavelength catalog available for the two CANDELS fields, which have 18/19 bands on UDS/GOODS, from U band to 8 μm. The SED technique employed for this work has been already intensively tested in previous papers (Fontana et al. 2003, 2004, 2006; Grazian et al. 2006; Santini et al. 2012). It is based on the comparison between the observed multi-color SED of each galaxy with those obtained from a set of reference synthetic spectra from stellar population models. The redshift of each galaxy is fixed to the spectroscopic or the photometric one during the fitting process.

Table 1. Parameters used for the library of template SEDs.

IMF	Salpeter
SFR τ (Gyr)	0.1, 0.3, 0.6, 1, 23, 4, 9, 15
log (age) (yr)	7, 7.01, 7.03...10.3
Metallicities	0.02 $Z_\odot$, 0.2$_\odot$, 1$_\odot$, 2.5$_\odot$
E_{B-V}	0, 0.03, 0.06, 0.1, 0.15, 0.2, ..., 1.0
Extinction law	SMC, Calzetti

We decided in this case to use a fairly standard reference spectral library to facilitate comparison with results in the literature. It is based on the BC03 models, and the code was run using a Salpeter IMF, ranging over a set of metallicities from $Z = 0.02\,Z_\odot$ to $Z = 2.5\,Z_\odot$, and dust extinction A_V ranging between 0 and 1.0 assuming a Calzetti extinction curve. We used smooth, exponentially-decreasing star-formation histories. All the parameters adopted for the SED fitting are listed in Table 1. The best-fitting spectrum provides estimates of the star-formation rate (SFR), extinction, stellar population age (the onset of the star formation episode), galaxy stellar mass, and τ (the star-formation e-folding timescale).

Among the outputs of this analysis, we use in particular the stellar masses and the age/τ parameter, which is the inverse of the Scalo parameter. As shown in Grazian et al. (2007), this parameter can be used to distinguish between star-forming and passively evolving galaxies. Following their work, we assume age/$\tau < 4$ for the former and age /$\tau \geq 4$ for the latter.

3. *BzK* galaxies in CANDELS

3.1. Raw BzK counts

As first proposed by Daddi et al. (2004), the BzK color–color criterion is an efficient color-based method for identifying galaxies in the redshift range $1.4 < z < 2.5$. It also permits segregation of galaxies between actively star-forming galaxies (sBzK) and passively evolving galaxies (pBzK). If we define $BzK = (z-K) - (B-z)$, sBzK galaxies have colors consistent with $BzK > -0.2$, while pBzK galaxies have $BzK < -0.2$ and $(z-K) > 2.5$ (corresponding to the upper left and upper right regions of the color-color diagram, respectively; see Fig. 1).

Figure 1 shows the $B-z$ versus $z-K$ distribution of $K \leq 24$ sources in the CANDELS GOODS-S (upper panel) and UDS (lower panel) fields. While all BzK galaxies are detected in the z-band images, the same does not hold for the B band, where several of them are undetected even in our ultradeep images. For these sources we assume a lower limit on B-band magnitude that is equal to their 1σ limiting magnitude and plot them in Fig. 1. We note that, in principle, BzK galaxies undetected in the B band and located in the sBzK region could be pBzK galaxies scattered leftward into the sBzK region, as shown also in Grazian et al. (2007), which therefore escape inclusion in the pBzK sample.

Based on our sample, we are able to compute the raw number counts derived for both the sBzK and pBzK galaxies in the CANDELS fields for both fields separately, as shown in Fig. 2. The error bars are computed assuming Poisson statistics, approximated with the square root of the counts for $N > 10$ and the small-number approximation for the Poisson distribution of Gehrels (1986) for $N \leq 10$. It is immediately clear that our observations reach a depth that no previous studies have achieved. Also evident is the decrease in the number counts of pBzK galaxies at magnitudes fainter than $\simeq$21.5–22. To establish whether

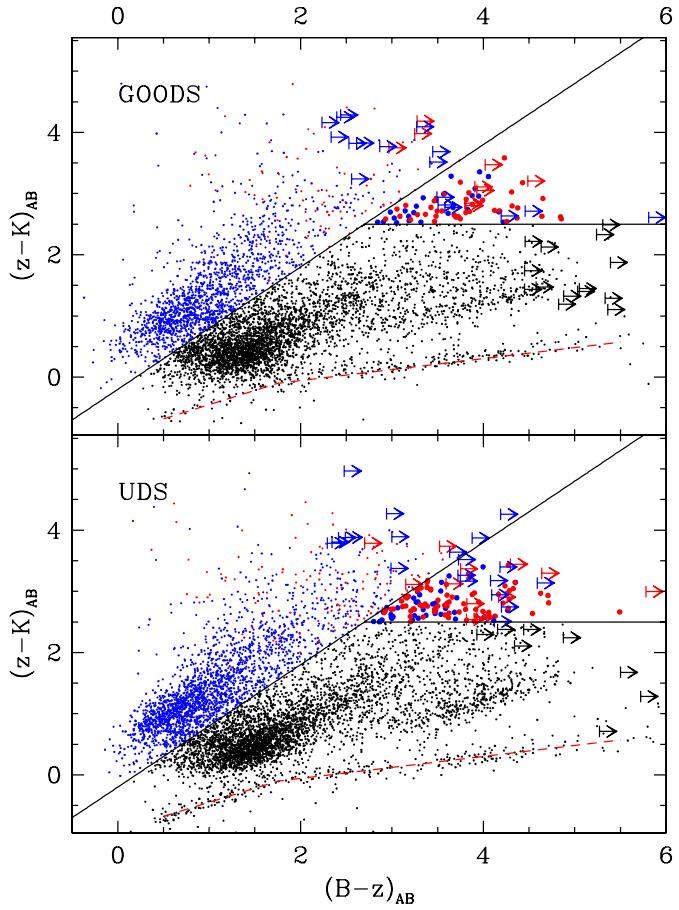

Fig. 1. $B-z$ versus $z-K$ color–color diagram for the K-selected galaxies and stars in the CANDELS GOODS-S (*upper panel*) and UDS (*lower panel*) fields. Arrows indicate 1σ lower limits on the measured $(B-z)$ color for sources that are undetected ($S/N < 1$) in the B band. Objects shown in blue are color-selected BzK galaxies classified as "star-forming" from the SED analysis. Those plotted in red are color-selected BzK galaxies classified as passively evolving with the same criterion. The red dashed line is a fixed reference to show the position of stars in the BzK plane, useful for showing the consistency of photometric calibration.

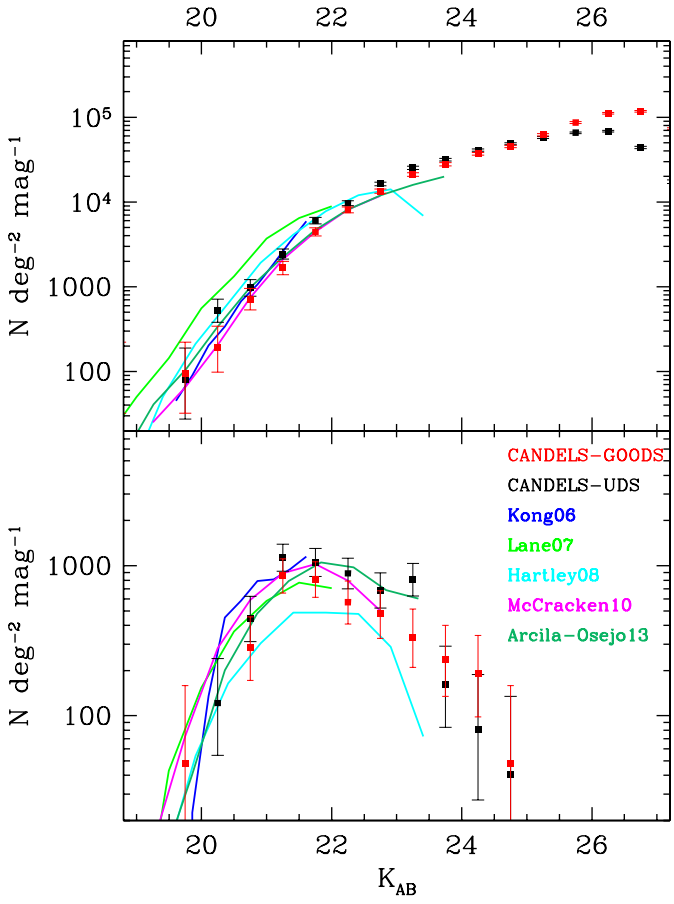

Fig. 2. Number counts for the sBzK (*upper panel*) and pBzK (*bottom panel*) galaxies in the two CANDELS fields plotted separately, red GOODS-S and black UDS. We assume Poissonian error bars, computed with the Gehrels (1986) formula for low number counts. Previous results from the literature are overplotted: Kong et al. (2006) in blue, Lane et al. (2007) in green, Hartley et al. (2008) in cyan, McCracken et al. (2010) in magenta, and Arcila-Osejo et al. (2013) in dark green.

this turnover is real we performed dedicated simulations that are described in the following section.

The number counts for star-forming and passive BzK galaxies are reported in Tables 2 and 3, respectively. Since the detection is made on the deep H-band CANDELS images, the number counts for the sBzK extends well below $K \simeq 27$, where they are, however, significantly plagued by incompleteness in the detection. Since we are interested here in the pBzK population, which is limited at much brighter magnitudes by incompleteness due to color selection, as we quantify below, we have made no attempt to correct for the detection incompleteness in the faintest bins of the sBzK counts.

As far as sBzK galaxies are concerned, our number counts are in reasonable agreement with most of the previous studies, encompassing the range of densities found by previous works, which typically were conducted over much larger areas. Probably the most striking difference is with respect to Lane et al. (2007), whose counts are above our own (and all the others). As proposed by McCracken et al. (2010), this difference could be due to an inappropriate transformation to the Daddi et al. filter set. However, we also note that they have been obtained over the UDS region. As shown in Fig. 2, our counts

Table 2. Observed number counts of sBzK and pBzK galaxies in the UDS and GOODS-S fields, separately.

K_{AB}	$N_{sBzK-UDS}$	$N_{sBzK-GOODS}$	$N_{pBzK-UDS}$	$N_{pBzK-GOODS}$
17.75	0	1	0	0
18.25	0	1	0	0
18.75	0	0	0	0
19.25	0	0	0	0
19.75	2	2	0	1
20.25	13	4	3	0
20.75	24	15	11	6
21.25	60	35	28	18
21.75	149	93	26	17
22.25	239	169	22	12
22.75	404	282	17	10
23.25	625	441	20	7
23.75	778	586	4	5
24.25	1012	776	2	4
24.75	1207	945	1	1
25.25	1421	1302	0	0
25.75	1623	1816	0	0
26.25	1690	2342	0	0
26.75	1089	2471	0	0

Notes. The total averaged number counts, including also a completeness correction, are given in Table 3. The first column shows the center of each 0.5 mag bin.

Table 3. Differential number counts for sBzK and pBzK averaged over the (UDS+GOODS-S) fields.

K_{AB}	N_{sBzK}	N_{pBzK}	N^{Corr}_{pBzK}
19.75	$1.817^{0.30}_{0.35}$	$1.340^{0.52}_{0.87}$	$1.327^{0.52}_{0.87}$
20.25	$2.570^{0.12}_{0.12}$	$1.817^{0.30}_{0.35}$	$1.813^{0.30}_{0.35}$
20.75	$2.920^{0.08}_{0.08}$	$2.570^{0.12}_{0.12}$	$2.563^{0.12}_{0.12}$
21.25	$3.304^{0.05}_{0.05}$	$2.993^{0.07}_{0.07}$	$2.987^{0.07}_{0.07}$
21.75	$3.696^{0.03}_{0.03}$	$2.931^{0.07}_{0.08}$	$2.930^{0.07}_{0.08}$
22.25	$3.935^{0.02}_{0.02}$	$2.871^{0.08}_{0.08}$	$2.879^{0.08}_{0.08}$
22.75	$4.165^{0.02}_{0.02}$	$2.738^{0.09}_{0.10}$	$2.755^{0.09}_{0.10}$
23.25	$4.354^{0.01}_{0.01}$	$2.755^{0.09}_{0.09}$	$2.811^{0.09}_{0.09}$
23.75	$4.461^{0.01}_{0.01}$	$2.294^{0.16}_{0.17}$	$2.431^{0.16}_{0.17}$
24.25	$4.579^{0.01}_{0.01}$	$2.118^{0.20}_{0.22}$	$2.473^{0.20}_{0.22}$
24.75	$4.661^{0.01}_{0.01}$	$1.641^{0.37}_{0.47}$	$2.565^{0.37}_{0.47}$
25.25	$4.760^{0.01}_{0.01}$		
25.75	$4.860^{0.01}_{0.01}$		
26.25	$4.924^{0.01}_{0.01}$		
26.75	$4.873^{0.01}_{0.01}$		

Notes. The first column is the center of the bins. The remaining columns are in units of log(N/deg^2/mag) . The last column shows the pBzK counts after correction for incompleteness and contamination, as described in the text.

in the UDS region are also above those in the GOODS-S region. It is therefore possible that some of this excess is due to a true overdensity of galaxies in the UDS field, where indeed a large number of $z \simeq 1.6$ galaxies within a high-density structure have been observed (Papovich et al. 2010; Tanaka et al. 2010). We also note that the mismatch between our two fields is close to the limit of what can be accounted for by a straightforward application of clustering statistics. Looking for instance at sBzK galaxies with $K \leq 22$, we find 151 and 248 galaxies in the GOODS-S and UDS fields, respectively. Using the Cosmic Variance Calculator (Trenti & Stiavelli 2008) to estimate their expected variance and converting their density to the same area of one square degree, we find that their densities are 3600 ± 596 galaxies per square degree and 5015 ± 707 galaxies per square degree, repectively, hence discrepant at the 2−3σ level.

Focusing our attention now on the main subject of the current paper, the number densities of pBzK galaxies in the two fields match the observed number densities from the literature in the bins where we have good statistics. There is some discrepancy with previous works, especially with McCracken et al. (2010) and Kong et al. (2006). This difference may be due to cosmic variance, given the strong clustering of pBzK galaxies with respect to sBzK galaxies. There is also a systematic difference between our two fields: in total, we identify 134 pBzK galaxies in the UDS and 81 in GOODS-S, and even in this case, the UDS field seems overdense. Following the Cosmic Variance Calculator as described before, this translates into a number density of 1930 ± 380 and 2710 ± 440 in the GOODS-S and UDS fields, respectively, which is still consistent within 2σ.

3.2. The redshift distribution of BzK galaxies

Both the UDS and the GOODS-S fields have been the target of extensive spectroscopic surveys in the past. Using these publicly available data, we first verified the accuracy and completeness

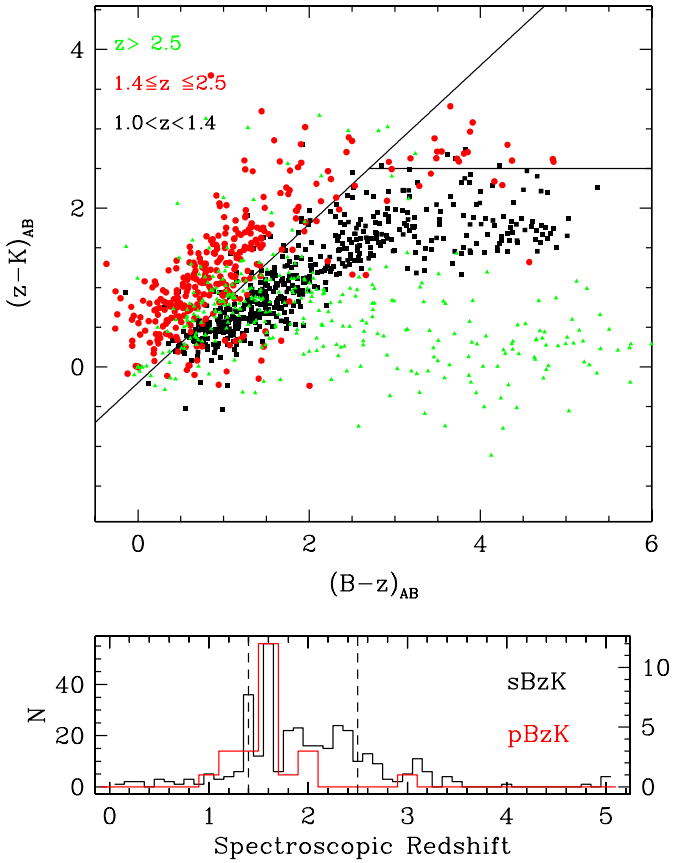

Fig. 3. BzK with spectroscopic redshift. *Upper panel*: position of all galaxies with $z_{spe} > 1$ on the BzK plane. Each symbol refers to a different redshift range, as shown in the legend. *Lower panel*: the spectroscopic redshift distribution for the BzK galaxies, divided between sBzK and pBzK, as shown in the legend. The vertical dashed lines represent the canonical redshift range of BzK galaxies.

of the BzK selection criteria in selecting galaxies in the redshift range $1.4 < z < 2.5$, expoiting a sample that is significantly larger than the original K20 sample used by Daddi et al. (2004). This is shown in Fig. 3, where we plot the position of all sources with spectroscopic redshift $z_{spe} > 1$ in the BzK diagram; each symbol refers to a different redshift range. Figure 3 also shows the distribution of the spectroscopic redshifts of these BzK-selected galaxies. The significant overlap between the $1.4 < z < 2.5$ galaxy population and the BzK selection criterion is immediately evident. More quantitatively, we find that within the spectroscopic sample, 318 galaxies (38 & 280 in the UDS and GOODS-S, respectively) fall in the sBzK region. Of these, 225 (23 & 202) are at $1.4 \leq z \leq 2.5$. The total number of pBzK galaxies with spectroscopic redshifts is 15 (1 & 14), with only two of them outside of the $1.4 \leq z \leq 2.5$ redshift range. Conversely, 56 galaxies (2 & 54) at $1.4 \leq z \leq 2.5$ are not in the overall BzK region. Based on these numbers, we conclude that the completeness of the BzK selection criterion is about 80% and the purity around 70%. We have also verified that these numbers drop very significantly as soon as we move below $z = 1.4$ or above $z = 2.5$. This comparison confirms that the BzK criterion is a very effective method of selecting galaxies in the specific redshift range $1.4 < z < 2.5$.

Despite the extensive spectroscopic coverage, we must rely on the accurate photometric redshifts to estimate rest-frame properties like stellar mass for 95% of our BzK sample. The resulting picture is shown in Fig. 4, where we plot both the photometric redshift and the stellar mass of all BzK galaxies as a

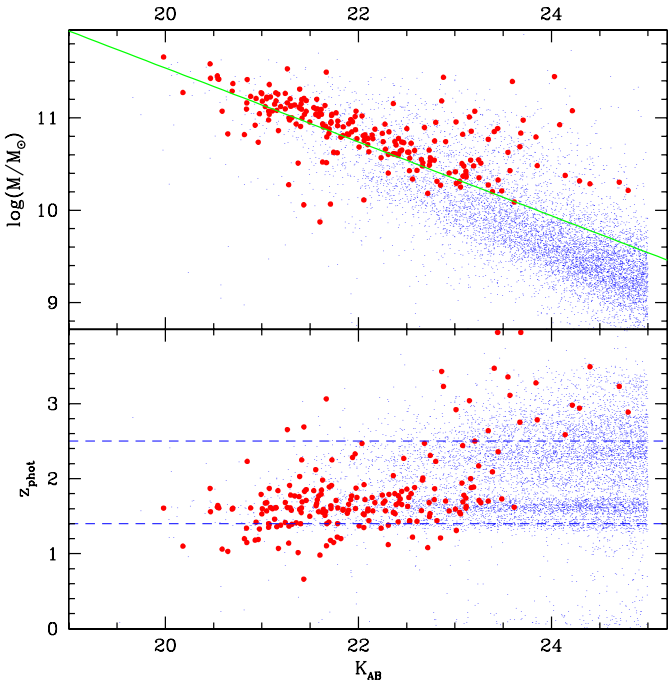

Fig. 4. Distribution of photometric redshift and stellar masses (*upper panel*) as a function of the K magnitude for the whole BzK sample. Blue small points refer to sBzK galaxies, red dots to pBzK. In the *lower panel* the two dashed lines represent the nominal redshift range of the BzK distribution; in the *upper panel*, the green thick line represents the average $M_{\odot} - K$ relation of Daddi et al. (2004).

function of their K magnitude. The two fields are shown together. It is easily appreciated that most of the pBzK galaxies have photometric redshifts below $z = 2$, with a $z_{\rm med} \simeq 1.8$, while the distribution of sBzK spans a wider range with $z_{\rm med} \simeq 1.9$. The redshift distribution of the passively evolved galaxies is in good agreement with the one presented in McCracken et al. (2010). We note that the peak of galaxies around $z \sim 1.6$ could be related to large-scale structures known in both UDS (Papovich et al. 2010; Tanaka et al. 2010) and GOODS-S fields (Castellano et al. 2007; Kurk et al. 2008).

The central point of Fig. 4, however, is the evidence that the majority of the faint pBzK galaxies – those at $K > 23$ – are located at $z_{\rm phot} > 2.5$, at variance with the brighter $K < 23$ sample, which are as expected at $1.4 < z < 2.5$. We inspected these sources individually and found that their photometry is not corrupted, and their photometric redshifts are reasonably well constrained. We note that the presence of passively evolving galaxies in the pBzK region does not contradict the expectations of synthesis models. The BC03 spectral library described before predicts that passively evolving galaxies at $z > 2.5$ may also be located in the pBzK area.

It is also interesting to look at the stellar mass estimates for the BzK population. As shown in the upper panel of Fig. 4, both pBzK and sBzK follow a general trend between the K-band and the stellar mass $M_{\odot}$. Indeed, Daddi et al. (2004) derived an average relation between K-band magnitude and the stellar mass of the form $\log(M_{\star}/10^{11}\ M_{\odot}) = -0.4(K^{\rm tot} - K^{11})$, where $K^{11} = 21.35$ (AB) is the K-band magnitude corresponding to a mass of $10^{11}\ M_{\odot}$ on average. This was calibrated on the stellar mass estimates derived from full SED fitting in the K20 spectroscopic sample (Fontana et al. 2004), i.e. on galaxies with $K_{\rm AB}$-magnitude less than 22, where exactly the same numerical code as adopted here was used to estimate masses, although a previous version of the BC03 code was adopted. This is shown in Fig. 4. The superior quality and spectral extension of the CANDELS imaging data gives us the opportunity to revise such a relation. While the Daddi et al. (2004) relation seems to represent the correlation for bright sources fairly, we find that it systematically overpredicts the stellar mass for fainter sources. This is consistent with expectations considering that faint sBzK are typically low-mass star-forming galaxies, whose M/L is expected to be lower than more massive, evolved galaxies.

It is interesting to note that the faint pBzK galaxies that we locate at $z > 2.5$ are significantly offset from the general relation, as expected since they are at considerably higher redshifts.

4. Estimating the systematic effects

4.1. Incompleteness

As is evident by looking at Fig. 2, the number counts of pBzK galaxies drop at fainter magnitudes beyond $K \simeq 21.5$. Since this is the main focus of the present paper, it is important before analyzing it in more detail to exclude the possibility that this behavior is due to systematics in the data. As already discussed in Sect. 2, we can exclude that blending is a major cause of photometric errors or that image inhomogeneities are a major source of incompleteness. It is certainly possible, however, that this effect is due to photometric scatter. The photometric scatter could be potentially troublesome in the case of the B band, which ultimately limits our pBzK selection at the faint end. To properly measure the $B - K$ color of a galaxy at the center of the pBzK region (e.g., with $(B - z) = 4$ and $(z - K) = 3$) , the B band must be deep enough to allow the detection of the object that is as much as $\simeq$7 mag fainter than the K-band magnitude of the object. Given the depth of our B-band ($B \simeq 30$ mag.), we expect that incompleteness is already important at $K \simeq 23$. Previous analyses used B-band images that were about two magnitudes shallower, so we can expect these effects to have been in place at even brighter magnitudes in those surveys. To verify this further, we performed the simulations described below.

The effects of noise and incompleteness can affect the observed distribution of galaxies in various ways in the BzK plot. First, photometric noise may scatter galaxies within the BzK diagram; in particular, galaxies that lie close to the lines that define the selection criteria can migrate in or out of the selection windows. In the case of the horizontal line at $z - K > 2.5$, the exquisite depth of the CANDELS and HUGS data is crucial for keeping these effects to a minimum. For instance, at $K = 24$ in the GOODS-S field, the typical error on the K-band magnitude is $\simeq$0.05 mag, and the color term $z - K = 2.5$ is measured with a total error of typically 0.2 mag. (We emphasize that all the pBzK galaxies are detected in the z-band.) The diagonal selection line is more affected by the depth of the B-band image. Again, the depth of the B band (the 1σ detection limit is $B \simeq 30$ in both fields) ensures detection also in the B-band for a large number of the pBzK galaxies down to $K = 24$. Those that were not detected are shown in Fig. 1: those lying outside the pBzK region could in principle bona fide pBzK galaxies scattered out because of the inadequate depth of the B band.

Clearly, the opposite effect may also happen. Galaxies located outside the boundaries of the pBzK criterion can enter the region because of photometric noise and be included in the pBzK galaxy sample. To quantify these effects in our samples, we performed a dedicated set of simulations. The ultimate goal is to define a robust limiting magnitude in the K band and to correct a posteriori the observed number counts for *incompleteness* (i.e.,

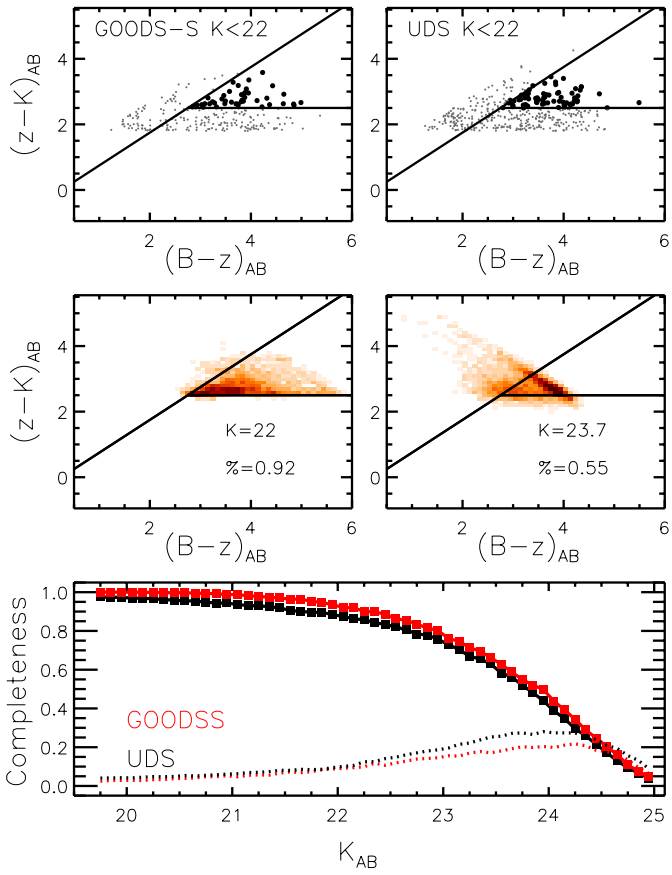

Fig. 5. Simulations used to estimate the completeness in the selection of pBzK galaxies. *Upper panel*: position of the sources used to estimate the incompleteness in the two fields, taken as real pBzK galaxies at $K < 22$. *Central panels*: example of the density of simulated sources in the BzK plane, when sources are scaled to $K = 22$ (*left*) and $K = 23.7$ (*right*), and when the effect of noise is included (see text for details). The case of GOODS-S is shown in this example. *Lower panel*: big dots delineate the completeness (i.e., the fraction of objects originally located in the pBzK region that are recovered even when the appropriate photometric noise is included) as a function of the K-band magnitude resulting from the full simulations, separately for the two fields. The small dots show the contamination, i.e., the fraction of objects detected in the pBzK region that were originally located outside the same region.

the fraction of true pBzK galaxies lost due to noise) and *contamination* (i.e., the fraction of galaxies selected by the pBzK criterion that were instead originally located outside it).

The procedure that we followed is described in Fig. 5. To estimate the incompleteness, we started from the sample of observed pBzK galaxies, using the brightest part of the catalog, where observational errors are so small that they do not significantly contribute to the observed scatter. After inspecting the error budget in the input catalogs, we decided to use all objects with $K < 22$ for this purpose. Similarly, we used the observed catalog of objects with $K < 22$ and located in a region around the pBzK boundary to estimate the amount of contamination in our sample. This sample is shown in the upper panel of Fig. 5, where we plot the distribution of the objects used as input in the BzK plane, which is slightly different in the two fields. We show both the galaxies selected as input pBzK galaxies, as well as those lying immediately out of the pBzK region used to estimate the contamination.

We used these objects to generate mock catalogs of 10^5 objects for each field, normalized at various K-band magnitudes from $K = 20$ to $K = 25.5$. The computed magnitudes (in all bands) are then perturbed by assigning them a noise consistent with the observed error-magnitude relation in each band and field. Our simulations accurately reproduce not only the average signal-to-noise ratio (S/N) as a function of magnitude, but also its scatter in order to match the observed and simulated data as closely as possible (Castellano et al. 2012).

Both these catalogs are then analyzed in a similar way to the ones derived from the observations. The output of this exercise is shown in the central panel of Fig. 5, where we plot the position of the simulated catalogs after applying the noise, for pBzK galaxies only, in the case of two reference magnitudes ($K = 22$ and $K = 23.7$). For simplicity we plot only the GOODS-S field.

This plot clearly shows the effect of the finite depth of our observations. As galaxies become fainter, there is some scatter across the $z - K = 2.5$ boundary, which is, however, relatively small. By far the stronger effect is the migration of objects toward smaller $B - z$ onto the clear locus of galaxies with undetected B-band flux. This effect clearly depends on the object flux and removes a significant fraction of objects from the pBzK region. Similar results (not shown in the figure) are found for the contamination, where the primary effect is due to photometric noise that causes objects close to the boundaries to enter the pBzK region.

The final results are shown in the lower panel of the same Fig. 5, where we plot both the completeness and the contamination as a function of the K-band magnitude. They have been computed separately for the two fields, which have slightly different depths in the various bands. We find that the incompleteness obviously increases with increasing magnitude, since it is relatively small (<20%) up to $K = 22.5$–23 but reaches a level of 50% at about $K = 23.5$ for UDS and $K = 24$ for GOODS-S. In the following we therefore focus our analysis on the $K < 24$ sample and simply present our results down to $K = 25$, warning the reader that incompleteness corrections are very severe at $K > 24$. The contamination also increases at the faint end of our sample, reaching 20–25% at $K \simeq 24$. We use these curves in the following to correct our number counts.

4.2. Spectral classification

We also compared the galaxies selected with the simple color-selection criteria to the output of a full SED analysis, performed on the multiwavelength catalogs obtained from CANDELS. To understand the limitations of the BzK selection criterion, derived only from observed colors, we follow a different approach based on the spectral fitting technique. One simple test to verify the validity of the BzK criterion is to analyze the population of BzK galaxies by correlating the age t, the star-formation timescale τ, and the dust extinction $E(B - V)$ derived from the SED fitting technique already described in Sect. 2.3.

As in Grazian et al. (2007), for each galaxy we computed the t/τ parameter, and we characterize as star-forming the galaxies with $t/\tau < 4$, and those with $t/\tau \geq 4$ as passively evolving. We therefore first verified that the classification based on the t/τ parameter is consistent with the results obtained using the BzK criteria; i.e., we computed this parameter for all the BzK galaxies, and for all of them we examined the correlation between t/τ and the extinction. We verified that both star-forming and quiescent galaxies have the expected value of t/τ, as for the extinction. As shown in Fig. 1, there is a general consistency between the position in the BzK plane and the result of the SED fitting (we recall that the latter is obtained over 18–19 bands, not only on 3 as in the BzK case). Those located in the pBzK region are mostly

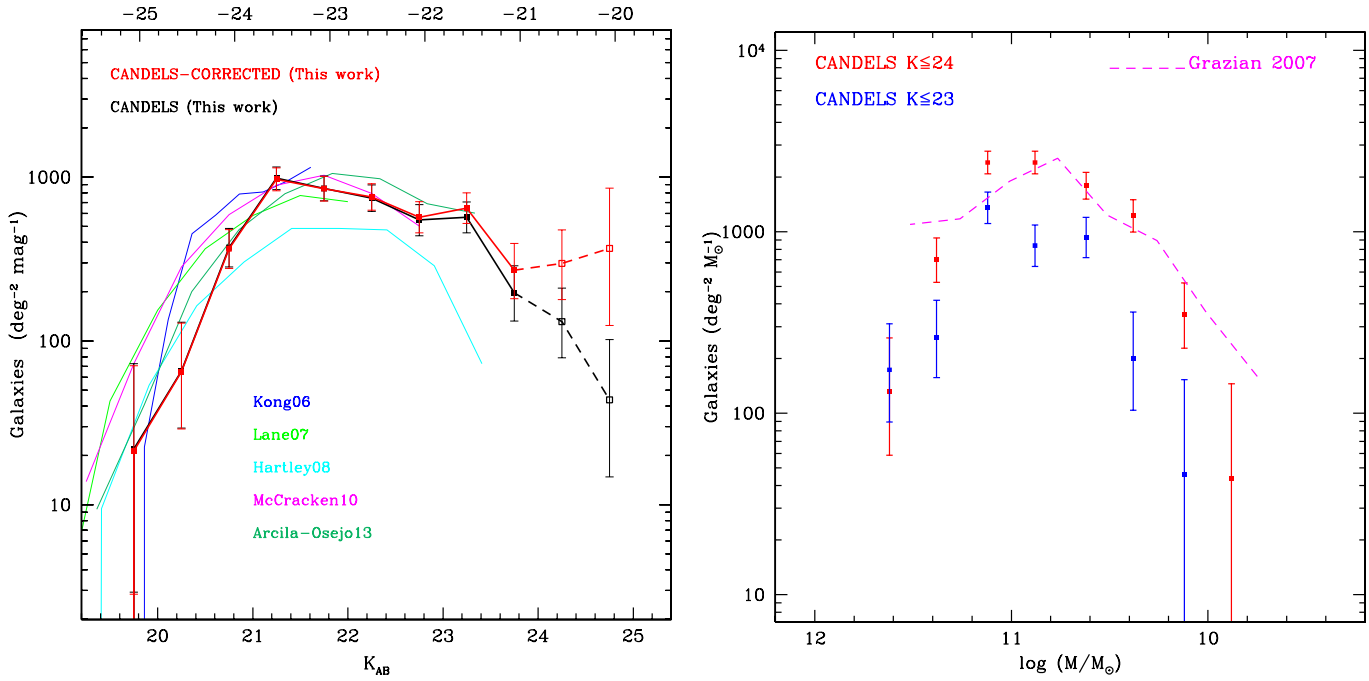

Fig. 6. *Left*: number counts of the CANDELS (UDS+GOODS-S) pBzK galaxies as a function of the observed K magnitude. The black points and line show the raw data, while the red points and line show the data after correcting for incompleteness as discussed in the text. The upper x-axis shows the corresponding rest-frame absolute magnitude in the I band at $z \simeq 2$. As highlighted in the text, the corrections for incompleteness are below a factor 2 at most up to $K \simeq 24$, which sets the limit for a rigorous analysis. However, we plot the faint end of the distribution until $K < 25$ with a dotted line for reference. The blue, green, cyan, magenta, and darkgreen lines show the number counts for pBzK galaxies from Kong et al. (2006), Lane et al. (2007), Hartley et al. (2008), McCracken et al. (2010), and Arcila-Osejo et al. (2013), respectively. *Right*: the stellar mass distribution of the CANDELS pBzK galaxies, after correction for incompleteness and contamination as described in the text. Masses are obtained with the multiband SED-fitting technique. Blue points are obtained from the $K < 23$ sample, where all galaxies are at $z < 2.5$, while the red points are from the $K < 24$ sample, which includes objects up to $z \simeq 3.5$. For comparison we also plot the galaxy stellar mass distribution of the pBzK derived by Grazian et al. (2007) from the GOODS-MUSIC sample (magenta dashed line).

fitted with passively evolving models, while those located in the sBzK area are fitted with star–forming models. This supports our conclusion that a relatively low number of pBzK galaxies are scattered out of the pBzK region because of limited depth of the B-band imaging.

5. Passively evolving *BzK* galaxies: luminosity and mass distribution

Armed with full characterization of the selection function, we are now in a position to explore the properties of the pBzK galaxies. Figure 6 presents the K-band number counts of the pBzK galaxies in the CANDELS fields. In addition to the raw counts, when averaged over the two fields, we present the number counts, corrected for incompleteness, up to $K = 24$. For this purpose each galaxy of magnitude K in the sample has been summed as $[1 - contamin(K)]/complet(K)$, where $contamin(K)$ and $complet(K)$ are the contamination and completeness as defined above and as shown in the lower panel of Fig. 5. Error bars are Poissonian and computed as described above. For comparison, we also overplot the number counts found by Kong et al. (2006), Lane et al. (2007), Hartley et al. (2008), and McCracken et al. (2010) that were not corrected for incompleteness. The number counts are in good agreement with previous studies at faint magnitude. The pBzK galaxy number counts derived from our CANDELS (UDS+GOODS-S) sample are summarized in Table 3.

When the correction is applied, the observed number counts still show a flattening at $K > 21$, consistent with past studies (e.g., Hartley et al. 2008). The turnover at $K \simeq 22$ is still present, although somewhat less significant. After converting these magnitudes to average rest-frame magnitudes in the I band (which is sampled by the K band at $z \simeq 1.9$, close to the average redshift of pBzK galaxies with spectroscopic redshift), this corresponds to absolute magnitudes of $M_I \simeq -23$ and $M_I \simeq -22$, respectively, as shown by the upper x-axis in Fig. 6.

To investigate the physical significance of this trend further, we translated the galaxy photometry into stellar mass. We computed the stellar masses using our SED fitting to the full multiwavelength catalogs available for the two fields, computed as described in Sects. 2.3 and 4.2. We remind the reader that we have adopted a Salpeter IMF here.

Figure 6 shows the resulting distribution of the stellar masses for the pBzK galaxy sample computed with the SED fitting technique. As shown in Fig. 4, the majority of pBzK galaxies at $K > 23$ appear to lie at $z > 2.5$, at variance with those at $K < 23$. We therefore plot the distribution at $K < 23$ and at $K < 24$ separately. For comparison, we overplot the results obtained by Grazian et al. (2007), which were obtained from the pBzK sample in the (less deep) GOODS-MUSIC sample using the same SED fitting technique. The two results are quite consistent.

The observed distribution shows that there is a clear decrease in the number density of passively evolving galaxies at stellar masses below $10^{10.8}\,M_\odot$. This trend departs significantly from the overall form of the galaxy stellar mass function at this redshift, which continues to rise steeply to much lower masses (e.g., Ilbert et al. 2013). We stress that this implies that the fraction of pBzK galaxies compared to all BzK galaxies, hence to most of

the galaxies at $z \simeq 2$, is large (~25%) at $M_* \simeq 10^{11}\,M_\odot$ and becomes minimal (~1%) at $M_* \simeq 10^{10}\,M_\odot$.

6. Comparison with semi analytical models of galaxy formation

In the previous sections we have highlighted the existence of a clear break in the luminosity and mass distributions of passive galaxies at $z \simeq 2$, with these objects becoming progressively rarer beyond an observed K-band magnitude of $K \simeq 22$. This turnover in the number counts can be translated into a mass threshold roughly placed around $10^{10.8}\,M_\odot$. This implies that the mechanisms that halted star formation in galaxies at high redshift have been more efficient (or statistically more frequent) in massive galaxies rather than in lower mass ones. It is interesting to investigate whether this basic feature is reproduced by theoretical models of galaxy formation.

We concentrate on four semi-analytical models (SAMs): Menci et al. (2008), Merson et al. (2013) (based on the SAM of Bower et al. 2006), Somerville et al. (2012), and Lu et al. (specifically, in the best fit case of the rendition described in Lu et al., 2013; see also Lu et al. 2011, 2012). These models vary both in the way they assemble the dark matter halos and in the prescriptions adopted for the various physical mechanisms involved in galaxy formation. Here we briefly mention the physical processes relevant to discussing our result. We refer the reader to the original papers for full details of the models and outline here only the major differences.

In the Menci model, the merging histories of dark matter halos are described through Monte Carlo simulations. The Merson model uses dark matter merger histories extracted from the Millenium simulation (Springel et al. 2005), while the Somerville and Lu models use the Bolshoi N-body simulations (see Klypin et al. 2011 for details). We note that the resolution of these N-body simulations in practice sets a lower limit to the mass (thus to luminosity) of the smaller galaxies traced in the simulations, hence to the depth of the luminosity distributions that we are presenting. Different modes for suppressing gas cooling in massive halos are implemented in the SAMs, either by artificially turning off the cooling of hot gas in halos above a tunable mass threshold (as implemented in the Lu model) or through including a specific model for AGN feedback. The latter can be either related to the active AGN phase (quasar mode) or ignited by the continuous accretion of gas in dark matter halos undergoing quasi-hydrostatic cooling (radio mode). The quasar mode is implemented in both the Somerville and the Menci models, which both assume that the AGN activity is triggered by galaxy interactions: the latter can only be constituted by galaxy merging (as in the Somerville model) or can include galaxy fly-by (as in the Menci SAM). The radio-mode AGN feedback is implemented in the Merson and Somerville models, and it influences galaxies with massive black holes at the center of massive halos.

All these models provide simulated galaxy samples, for which magnitudes in any desired filter set are given. The Somerville and Lu models provide lightcone mock catalogs that mimic the geometry of the UDS and GOODS-S fields, while the other two are averaged over larger areas of the sky. Galaxy magnitudes are computed from the predicted star formation and chemical enrichment histories using the single stellar population model (SSP). All these models use the SSP model of Bruzual & Charlot (2003), but they assume a different initial mass function (IMF): Kennicutt IMF (Merson), Salpeter IMF (Menci), and Chabrier IMF (Somerville and Lu). We do not correct the luminosities and colors for the different IMFs because the parameters of each model have been tuned to reproduce observations.

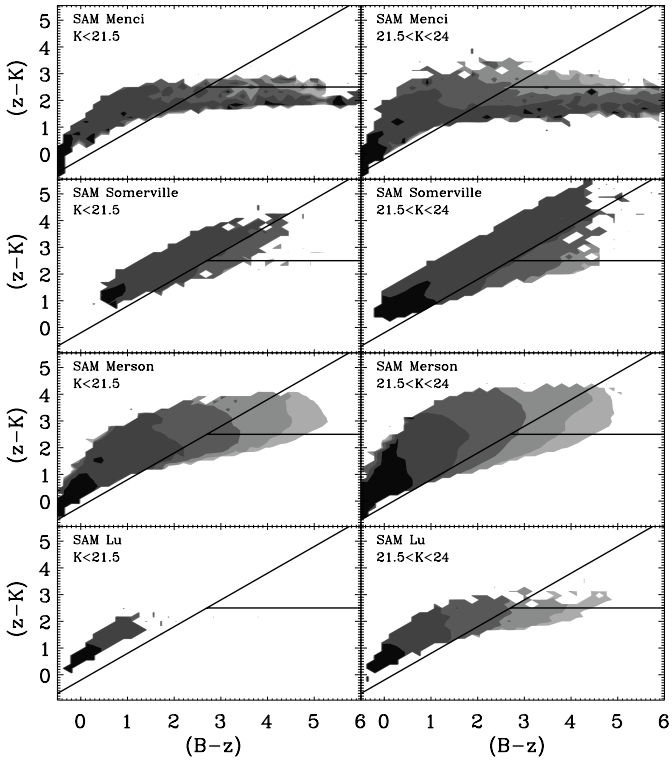

Fig. 7. $B-z$ versus $z-K$ color–color diagram for model galaxies in two bins of K-magnitude. The filled contours correspond to the predicted average values of the specific star-formation rate of model galaxies for bins of different B-z and $z-K$. The SSFR values are equally spaced on logarithmic scale from $SSFR = 10^{-13}$ yr^{-1} for the lightest filled region to $SSFR = 10^{-9}$ yr^{-1} for the darkest.

The dust extinction affecting the above magnitudes is computed from the dust optical depth and applying the appropriate attenuation to the luminosity at various wavelengths. The only exception is the Lu et al. model that does not include dust extinction. For all these models we extracted the BzK magnitudes and applied exactly the same BzK criterion as we applied to real data, as described in the previous sections.

First of all we tested whether these models are able to reproduce the passive galaxies selected by the pBzK criterion. To this aim, Fig. 7 shows the distribution of model galaxies at $1.4 < z < 2.5$ in the BzK plane in two bins of K magnitude, one corresponding to K magnitudes below the observed peak in the number counts at $K \simeq 21.5$, the other corresponding to fainter magnitudes. The grayscale shows the average specific SFR (SSFR) at a given position in the BzK plane, in decades ranging from quiescent galaxies ($SSFR = 10^{-13}$ yr^{-1}) to actively star-forming ($SSFR = 10^{-9}$ yr^{-1}). All models reproduce the distribution of galaxies in the BzK diagram reasonably well. On average, the SSFR of galaxies populating the upper right region of the $B-z$ versus $z-K$ color plane is lower than it is in those populating the BzK star-forming region ($BzK \geq -0.2$). In the case of the Menci model, there is a fairly large fraction of objects slightly outside the BzK region, but this is still consistent with the expected color evolution of galaxies at various ages in the redshift range $1.4 < z_{\rm phot} < 2.5$ (Daddi et al. 2004). The Lu et al. model is devoid of bright sBzK galaxies in the reddest region ($(B-z) \simeq (z-K) \simeq 2$). This region is mostly populated

by dusty star-burst galaxies, so this deficit is expected, considering that the Lu et al. model does not include a prescription for dust absorption. In particular, in all models, the pBzK criterion selects galaxies with $SSFR < 10^{11}$ yr^{-1}, which is well below the inverse of the Hubble time at $z = 2$ ($1/t_{\rm Hubble} = 3 \times 10^{-10}$ yr^{-1}), thus the selected pBzK galaxies are actually passive (see, e.g., Franx et al. 2008; Fontana et al. 2009).

Most models do predict that some fraction of the population of passive galaxies at $z \simeq 2$ is actually located outside the classical pBzK region, such that present observations might be missing a whole class of objects in the color-color plane. As shown in Daddi et al. (2004) and in Grazian et al. (2007), the pBzK selection criterion primarily selects galaxies that have been passively evolving for about 1 Gyr: lowering the threshold in $(z - K)$ corresponds to introducing passive galaxies that are progressively younger, so they become more numerous. We should therefore expect that lowering this threshold would also increase the number of observed galaxies. Unfortunately, this cannot be easily checked in the data, since lowering the threshold in $(z - K)$ immediately also introduces galaxies at lower redshift that contaminate the selection.

This allows us to turn back to our central result for the decrease in the number density of passive galaxies at faint luminosities. We compare in Fig. 8 the predicted and observed number counts of pBzK galaxies as a function of K magnitude. Since the observations of pBzK galaxies are severely affected by incompleteness, we decided to follow a twofold approach. In the upper panel, we plot the comparison between the observed data and the theoretical data, including the effect of incompleteness in the theoretical data alone. The catalog produced by the theoretical models has been convolved with the instrumental noise as in the simulations used for estimating the completeness. In the lower panel, we have plotted the data corrected for incompleteness and the theoretical models with no correction. As expected, the two approaches provide us with a consistent picture, with the latter also giving us the opportunity to show what the models predict at magnitudes fainter than our survey.

We first note that two models, Merson et al. (2013) and Somerville et al. (2012), exhibit a general trend that is qualitatively consistent with the observed break in the luminosity distributions. Their predicted number density reaches a peak at $K \simeq 21.5$, similar to what we observe in the real data, and decreases at fainter magnitudes. However, they overpredict the absolute number density of the passive galaxies at faint magnitudes. By contrast, the Menci and the Lu models perform poorly both at high and at low masses. They underestimate the number of massive passive galaxies, do not even predict a turnover. In both cases the number counts continue to increase exponentially toward fainter magnitudes (i.e., to lower stellar masses).

These discrepancies highlight that some of the prescriptions adopted to describe the main baryonic processes lead to noticeable differences among the various models and in some cases need a substantial revision. We note that our criterion is effective at selecting galaxies that have been undergoing a passive phase since at least $\simeq$1 Gyr, already at $z \simeq 2$. This allows us to test the implementation of physical processes that not only quench the star-formation process but also prevents it from starting again after a relatively short time. In general terms, the formation of passive galaxies depends on several proceess, such as the efficiency of gas cooling and the star-formation rate, the ejection of gas out of galaxies (due for instance by AGN and stellar feedback), and processes that deplete their gas reservoir (like stripping of cold gas in halo merging). A higher efficiency in the star-formation process and a lower feedback lead to a fast

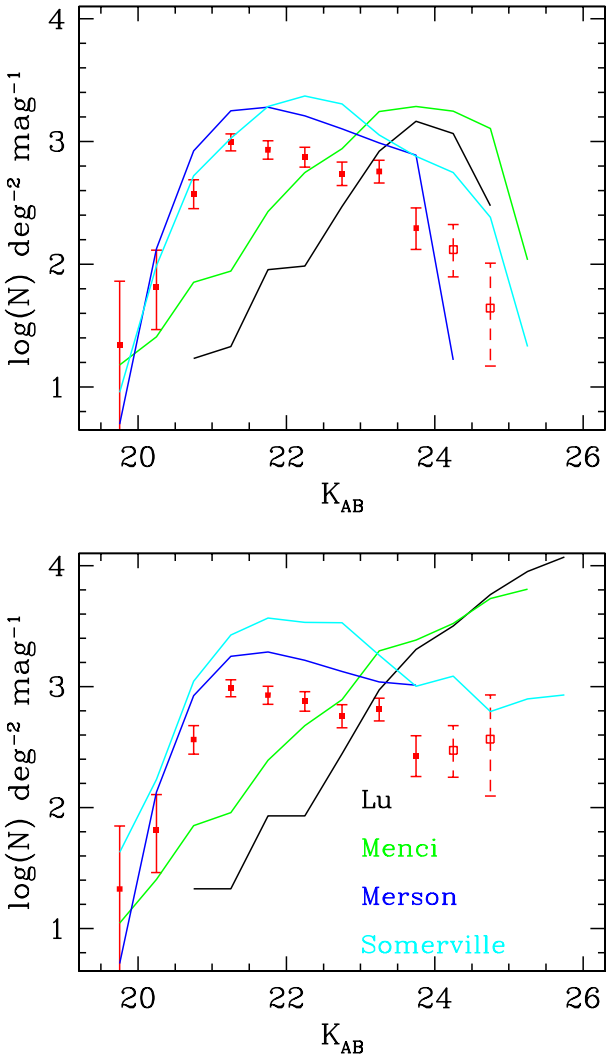

Fig. 8. Number counts of pBzK galaxies compared with model prediction of Merson et al. (2013) in blue, Menci et al. (2008) in green, Lu et al. (2013) in black, and Somerville et al. (2012) in cyan. *Upper panel*: mock catalogs from theoretical models (solid colored lines) are convolved with the same photometric errors and incompleteness as affect the data. Points refer to the raw observed counts without any correction for incompleteness. *Lower panel*: here the theoretical models are shown without any correction, while observed data are corrected for incompleteness as described in the text.

transformation of the gas content of a given halo into stars. In the absence of further cooling or in the presence of stripping of hot gas during halo merging, these processes makes galaxies quiescent. In contrast, lower efficiencies and higher feedback with subsequent cooling eventually lead to much more extended (albeit intermittent) epochs of star formation, making galaxies bluer. While these trends are common to all models, their specific implementation varies among them, leading to the differences that we observe.

At the bright magnitudes, the differences in model predictions can be interpreted in terms of the AGN feedback, which is often identified as a potentially major factor in the quenching of star-formation activity and is suspected to be more effective in massive galaxies. Based on this comparison, we can speculate that the radio mode feedback seems to be more efficient in producing bright passive galaxies than the QSO mode and halo-quenching model.

At faint magnitudes ($K \lesssim 23$), all models overestimate the number of passive objects. This is directly related to the well-known tendency of hierarchical clustering scenarios to produce steep luminosity functions (see, e.g., Somerville & Primack 1999; Cole et al. 2000; Menci et al. 2002; Benson et al. 2003). Hierarchical clustering scenarios predict that the high-redshift progenitor galaxies are characterized by low virial temperature and high densities, making the gas cooling extremely efficient at $z \gtrsim 3$. The short dynamical timescales and the frequent merging events rapidly convert this available cold gas into stars. In the absence of competing effects, the rapid star formation in low-mass galaxies at $z \gtrsim 3$ would result in an excess of red low-mass galaxies already at $z \simeq 2$, where our survey is sensitive.

Another physical process that is very important in predicting the number of faint red galaxies is the stripping of the hot gas reservoir of galaxies residing in subhalos. All models, indeed, assume that when a halo merges with a larger halo (becoming a subhalo), its hot gas content is stripped away. The galaxy residing in the subhalo rapidly consumes its cold gas reservoir and thereafter becomes red and passively evolving. This is particularly effective in dense environments at intermediate and high redshifts. The current implementation of such a mechanism produces an excess of red faint galaxies in all theoretical models developed so far. This aspect was explored at low redshift by Weinmann et al. 2006, comparing a SAM model to the observations from the SDSS survey. Guo et al. 2011 modified the implementation of the process in the model in order to delay the stripping of hot gas after halo merging. Even in this case, however, the excess of faint red galaxies is not completely removed. Other, more exotic possibilities have also been explored: for instance, Nierenberg et al. 2013 have shown that, by adopting a warm dark matter power spectrum, the number of satellite galaxies is significantly reduced.

There is no doubt that this excess is at least partly responsible for the excess of predicted galaxies that we observe at low masses in the pBzK population. For this reason Merson et al. (2013) made the test of removing the satellite galaxies completely from the predicted counts of pBzK, finding good agreement with the observed counts. This is clearly an indication that this process is involved in the overestimate. In the case of the Menci and Lu models the discrepancy at faint luminosities is much larger, even though gas stripping is included in a very similar fashion, suggesting that other processes are also involved. Unfortunately, it is impossible to make a more accurate test of the relative contribution of central and satellite galaxies, since some fraction of the observed data are also satellite galaxies, but given that extended large scale structures are detected in both our fields in the redshift range of BzK galaxies, this fraction could be substantial. This remains a clearly important test that deserves a dedicated analysis of the data (both in field surveys and in high-redshift clusters).

7. Summary and discussion

In this paper we have exploited new deep, wide-field K-band imaging, as performed with the High Acuity Wide field K-band Imager (HAWK-I) on VLT as part of the HAWK-I UDS and GOODS-S survey (HUGS; VLT Large Program), to study the population of passive evolving galaxies at $z \sim 2$. What is crucial is that both survey fields possess B and z-band imaging, as well as a wealth of other multiwavelength data, extending from the U-band to the mid-infrared *Spitzer* and containing deep HST imaging assembled as part of the CANDELS HST Treasury program.

To define a sample of star-forming and quiescent galaxies at redshift between $1.4 < z < 2.5$, we use the BzK criterion proposed by Daddi et al. (2004). Thanks to the depth of our observations, we have now extended the selection to magnitudes fainter than was possible in previous analyses. At bright magnitudes the observed number counts of the sBzK and pBzK galaxies are in good agreement with previous studies, in particular with McCracken et al. (2010) as shown in Fig. 2.

In particular we focus on passively evolving galaxies, the so-called pBzK galaxies. We find a total of 101 pBzK galaxies in the UDS CANDELS field and 89 in the GOODS-S field. We have demonstrated through simulations that – in our deep sample – the statistics of passive galaxies down to $K \simeq 22.5$ are not significantly affected by incompleteness and that the latter is still treatable down to $K \simeq 24$. Thanks to the depth of our observations, we are now able to place the earlier results on the pBzK number counts previously reported by Hartley et al. (2008) and McCracken et al. (2010) on secure footing.

Our central result is that the number counts of pBzK galaxies show a flattening at $K_s \sim 21$, with indications of a turnover at $K_s > 22$, equivalent to rest-frame absolute I-band magnitudes of $M_I = -23, -22$, respectively. Converted into stellar mass, our result corresponds to a decrease in the number density of passively evolving galaxies at stellar masses below $10^{10.8}\ M_\odot$ for a Salpeter IMF. As judged against the still steeply rising number counts of the overall galaxy population at these redshifts, this turnover is fairly abrupt, indicating that at high redshift the mechanism that quenches star-formation activity is much less efficient below this mass limit.

Another central result is related to the redshift distribution of pBzK galaxies. As expected, nearly all pBzK galaxies at $K < 23$ are at $1.4 < z < 2.5$. However, at $K > 23$ a sharp transition appears to exist, with most of the pBzK galaxies having a redshift definitely above $z = 2.5$, typically at $2.7 < z < 3.4$. This result confirms that there are passively-evolving galaxies at $z > 2.5$, as suggested by a number of recent papers (e.g., Fontana et al. 2009; Straatman et al. 2014).

We compared our observed number counts with the predictions of several semi-analytical models of galaxy formation and evolution, in particular with the models of Menci et al. (2008); Somerville et al. (2012); Merson et al. (2013); and Lu et al. (2011). Among these SAMs, only two, (Somerville et al. 2012; and Merson et al. 2013), qualitatively predict the shape of the number counts, showing a turnover at a stellar mass close to what is observed in the data, but they do not reproduce the absolute observed density of the passive galaxies. In contrast, the other two models fail to show this turnover and predict an exponential increase in passive objects to faint magnitudes. This comparison suggests that the distribution of number density (with magnitude or stellar mass) of quiescent galaxies at these redshifts offers a critical test for hierarchical models, and it can place strong constraints on the detailed baryonic physical processes involved in galaxy formation and evolution.

The importance of this basic finding should not be underestimated. Indeed, current models of galaxy formation are able to provide acceptable fits to the observed properties of the bulk of the galaxy population, such as luminosity functions or color distributions. What we show here is that the physical mechanisms that they implement are not able to correctly reproduce the extreme star-formation histories characterizing the pBzK galaxy population.

The observed discrepancies raise pressing questions concerning the comparison between observations and the current models of galaxy formation in a cosmological context. First,

are the current implementations of the star-formation quenching process (tuned to match the observed local luminosity functions) effective in reproducing the evolution of galaxies in the color-color plane? While at high masses the most likely candidate is the AGN feedback, at low masses, stellar feedback and gas stripping in satellite galaxies are probably the main processes that produce the observed abundance of the pBzK population. They both need to be better understood and parametrized to provide us with a satisfactory fit to the observed number counts.

Second, is the relative role of the different star-formation modes correctly implemented in the models? In particular, it is known that both merging and disk instabilities can provide star bursts that add to the secular conversion of gas into stars (the "quiescent mode" of star formation). Current galaxy-formation models are characterized by different implementations of three modes of star formation. While the bulk of the galaxy population could be less dramatically affected by the relative role of such processes, the abundance of pBzK galaxies characterized by extremely early star-formation histories could be extremely sensitive to the relative importance of the different star-formation modes.

Unfortunately, it is currently not possible to determine the specific features that produce the observed trends on the quenching of star formation within each model. This requires a more detailed investigation that we plan for a forthcoming paper.

Acknowledgements. We thank the referee, David Wilman, for a very useful report. The authors are grateful to the E.S.O. staff for their support during the Hawk-I observations. J.S.D. acknowledges the support of the Royal Society via a Wolfson Research Merit award, and also the support of the European Research Council via the award of an Advanced Grant. R.J.M. acknowledges the support of the European Research Council via the award of a Consolidator grant. A.F. and J.S.D. acknowledge the contribution of the EC FP7 SPACE project ASTRODEEP (Ref.No: 312725). This work is based in part on observations (program GO-12060) made with the NASA/ESA *Hubble* Space Telescope, which is operated by the Association of Universities for Research in Astronomy, Inc, under NASA contract NAS5-26555. This work is also based in part on observations made with the *Spitzer* Space Telescope, which is operated by the Jet Propulsion Laboratory, California Institute of Technology under NASA contract 1407. Program based in part on the data collected in the ESO programs 60.A-9284, 181.A0717, LP 186.A-0898 and 085.A-0961.

References

Andreon, S., & Huertas-Company, M. 2011, A&A, 526, A11
Arcila-Osejo, L., & Sawicki, M. 2013, MNRAS, 435, 845
Blanc, G. A., Lira, P., Barrientos, L. F., et al. 2008, ApJ, 681, 1099
Bower, R., G., Benson, A., J., Malbon, R., et al. 2006, MNRAS, 370, 645
Brammer, G.B., Whitaker, K. E., van Dokkum, et al. 2011, ApJ, 739, 24
Bruzual, G., & Charlot, S. 2003, MNRAS, 344, 1000
Calzetti, D., Armus, L., Bohlin, R., C., et al. 2000, ApJ, 533, 682
Castellano, M., Fontana, A., Grazian, A., et al. 2012, A&A, 540, A39
Daddi, E., Cimatti, A., Renzini, A., et al. 2004, ApJ, 617, 746
Daddi, E., Renzini, A., Pirzkal, N., et al. 2005, ApJ, 626, 680
Dahlen, T., Mobasher, B., & CANDELS Collaboration 2012, Am. Astron. Soc. AAS Meeting, 220, 133.01
De Lucia, G., & Blaizot, J. 2007, MNRAS, 375, 2
De Lucia, G., Springel, V., White, S. D. M., et al. 2006, MNRAS, 366, 499
De Lucia, G., Poggianti, B. M., Aragón-Salamanca, A., et al. 2007, MNRAS, 374, 809
Fioc, M., & Rocca-Volmerange, B. 1997, A&A, 326, 950
Fontana, A., Donnarumma, I., Vanzella, E., et al. 2003, ApJ, 994, 9
Fontana, A., Pozzetti, L., Donnarumma, I., et al. 2004, A&A, 424, 23
Fontana, A., Salimbeni, S., Grazian, A., et al. 2006, A&A, 459, 745
Fontana, A., Santini, P., Grazian, A., et al. 2009, A&A, 501, 15
Furusawa, H., Kosugi, G., Akiyama, M., et al. 2008, ApJ, 176, 1
Galametz, A., Grazian, A., Fontana, A., et al. 2013, ApJ, 206, 10
Gehrels, N. 1986, ApJ, 303, 336
Giavalisco, M., Ferguson, H. ,C., Koekemoer, A., M., et al. 2004, ApJ, 600, 93
Grazian, A., Fontana, A., Moscardini, L., et al. 2006, 453, 507
Grazian, A., Salimbeni, S., Pentericci, L., et al. 2007, A&A, 465, 393
Grogin, N. A., Kocevski, D. D., Faber, S. M., et al. 2011, ApJS, 197, 35
Guo, Q., White, S., Boylan-Kolchin, M., et al. 2011, MNRAS, 413, 101
Guo, Y., Ferguson, H. C., Giavalisco, M., et al. 2013, ApJS, 207, 24
Hartley, W. G., Lane, K. P., Almaini, O., et al. 2008, MNRAS, 391, 1301
lbert, O., McCracken, H., J., Le Fèvre, O., et al. 2013, A&A, 556, A55
Kitzbichler, M. G., & White, S. D. M. 2007, MNRAS, 376, 2
Klypin, A. A., Trujillo-Gomez, S., & Primack, J. 2011, ApJ, 740, 102
Kodama, T., Yamada, T., Akiyama, M., et al. 2004, MNRAS, 350, 1005
Koekemoer, A. M., Faber, S. M., Ferguson, H. C., et al. 2011, ApJS, 197, 36
Kong, X., Daddi, E., Arimoto, N., et al. 2006, ApJ, 638, 72
Lane, K. P., Almaini, O., Foucaud, S., et al. 2007, MNRAS, 379, 25
Lawrence, A., Warren, S., J., Almaini, O., et al. 2007, MNRAS, 379, 1599
Lee, K.-S., Ferguson, H. C., Wiklind, T., Dahlen, T., et al. 2012, ApJ, 752, 66
Lu, Y., Mo, H. J., Weinberg, M. D., & Katz, N. 2011, MNRAS, 416, 1949
Lu, Y., Mo, H. J., Katz, N., & Weinberg, M. D. 2012, MNRAS, 421, 1779
Lu, Y., Wechsler, R. H., Somerville, R. S., Croton, D. et al. 2013, ApJ, submitted [arXiv:1312.3233]
Menci, N., Fontana, A., Giallongo, E., et al. 2005, ApJ, 632, 49
Menci, N., Fiore, F., Puccetti, S., et al. 2008, ApJ, 686, 219
Merson, A. I., Baugh, C. M., Helly, J. C., et al. 2013, MNRAS, 429, 666
McCracken, H. J., Capak, P., Salvato, M., et al. 2010, ApJ, 708, 202
Muzzin, A., Marchesini, D., Stefanon, M., et al. 2013, ApJ, 777, 18
Nierenberg, A. M., Treu, T., Menci, N., et al. 2013, ApJ, 772, 146
Reddy, N. A., Erb, D. K., Steidel, C. C., et al. 2005, ApJ, 633, 748
Somerville, R. S., Gilmore, R. C., Primack, J. R., et al. 2012, MNRAS, 423, 1992
Straatman, C. M. S., Labbé, I., et al. 2014, ApJ, 783, L14
Stutz, A. M., Papovich, C., & Eisenstein, D. J. 2008, ApJ, 677, 828
Trenti, M., & Stiavelli, M. 2008, ApJ, 676, 767
Weinmann, S. M., van den Bosch, F. C., Yang, X., et al. 2006, MNRAS, 372, 1161